AD-A090 355 ARMY MISSILE COMMAND REDSTONE ARSENAL AL F/G 19/5
FREQUENCY DIVERSE TRACKING/GUIDANCE MILLIMETER RADAR ADAPTED TO--ETC(U)
JUN 80 P M ALEXANDER

UNCLASSIFIED NL

1 of 1
AD A
090355

END
DATE FILMED
11-80
DTIC

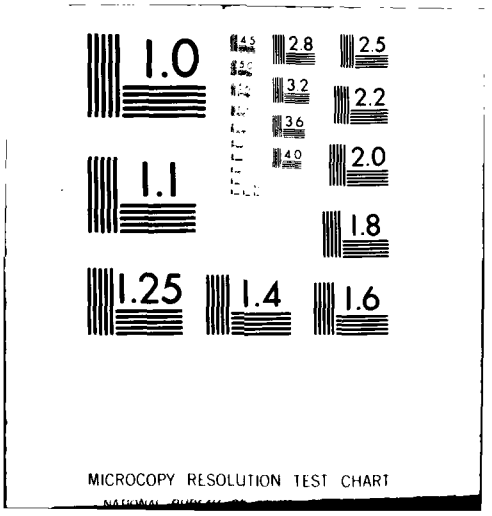
1.0
1.1
1.25
1.4
1.6
1.8
2.0
2.2
2.5
2.8
3.2
3.6
4.0
MICROCOPY RESOLUTION TEST CHART

FREQUENCY DIVERSE TRACKING/GUIDANCE MILLIMETER RADAR ADAPTED TO TARGET ACQUISITION

P. MARTIN ALEXANDER, PhD
US ARMY MISSILE COMMAND
REDSTONE ARSENAL, ALABAMA 35809

I. INTRODUCTION

Millimeter wave radar fire control for ground-to-ground tactical weapons provides a compromise between the resolution offered by electro-optical and infrared systems and the adverse environment (fog, battlefield smokes) penetrability which is characteristic of microwave systems. The effectiveness of millimeter sensors would be greatly enhanced if they could also be used to classify radar returns resulting from clutter, tanks, personnel carriers, etc., and particularly from stationary targets.

Missile fire control requires accurate target location, and, as a result, the use of frequency diversity has been investigated as a method of angle noise (glint) reduction to improve centroid tracking (1), (2), (3). Frequency diversity has more recently been examined as a tool for target acquisition (i.e., detection and classification) (4), (5), (6), (7), (8).

The detection/classification technique is based on: (1) the fact that, in general, targets and clutter consist of separate, individual reflectors distributed in range; and (2) the fact that the radar returns from any pair of reflectors will constructively or destructively interfere, depending on their separation in radar range and on the transmitted frequency. Thus, the basic measurement used in the acquisition technique is the radar response as a function of transmitted frequency.

It is hypothesized that the spacing in range for natural objects is more random than for manmade objects and, further, that manmade

objects have unique range spacings allowing discrimination of object classes. With this hypothesis, an analysis of frequency diverse radar returns is developed. The analysis is constrained by practical radar design parameters for a state-of-the-art, coherent, 142 GHz experimental radar, so that the analytical results can be experimentally tested. The analysis is also constrained to stationary targets and clutter.

Computer simulations are presented for a two-reflector target model and a three-reflector target model, and the analysis is extended to complications resulting from a chirped waveform. The applicability of the technique to real targets and clutter is considered. The parameters used for the analysis are: (1) a 3.0 microsecond pulse; (2) a 640 MHz frequency diverse bandwidth beginning at 142 GHz; (3) thirty-two frequency steps of 20 MHz for data acquisition; and (4) a linear frequency modulated chirp of 20 MHz for each pulse.

II. TWO-REFLECTOR TARGET MODEL

In the monostatic radar scenario depicted in Figure 1, the vertical, linearly polarized electric field incident on the i^{th} reflector can be written

$$E_i^t = E_o \cos\left[2\pi f(t-t_i/2)\right] \qquad t_i/2 \le t \le t_i/2 + T \tag{1}$$

where: f = radar frequency,
t_i = round trip echo time = $2R_i/c$, and
T = transmitted pulse length.

The echo, the electric field returned from the i^{th} reflector, at the receiver is given approximately by

$$E_i^r = \frac{\sqrt{\sigma_i}}{4\pi R_i^2} E_o \cos\left[2\pi f(t-t_i)\right] \qquad t_i \le t \le t_i + T \tag{2}$$

where σ_i is the radar cross section (RCS) of the reflector for vertical transmit and receive. Implicit in Equation (2) are the assumptions that the target is stationary, that the target reflectors are in the far-field of the radar, and that the radar is in the far-field of the reflectors. For antenna aperture D and characteristic reflector dimension a, the far-field region (Fraunhofer region) is given by

$$R_i > 2D^2/\lambda \qquad R_i > 2a^2/\lambda \quad \text{(for all } R_i\text{)} \tag{3}$$

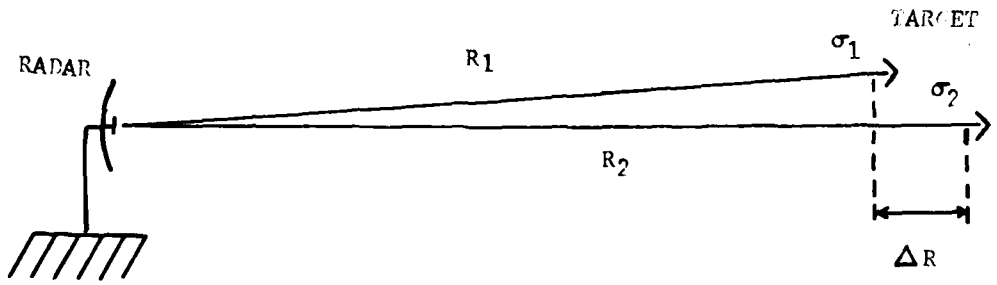

Figure 1. Radar/Target Scenario.

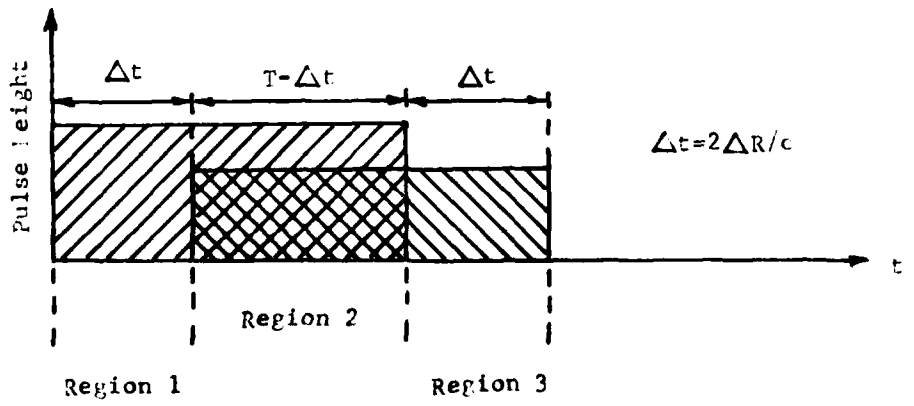

Figure 2. Arrival of Pulses from Two Reflectors ($\sigma_1 > \sigma_2$).

(91)

where λ is the transmitted wavelength.
It shall also be assumed for this analysis that $2\pi a \gg \lambda$ (optical region), and that the RCS of the reflectors vary as f^2, as for flat plates and corner reflectors.

For two reflecting centers on a target, the electric field strength at the antenna is

$$E^r = E_1^r + E_2^r \quad . \tag{4}$$

Figure 2 characterizes the arrival of the pulses at the antenna. In Region 2, the pulses overlap, resulting in constructive or destructive interference, depending on the relative phase. The electric field amplitude is given approximately by

$$E_m^r = \frac{E_o}{4\pi R^2}\left[\sigma_1 + \sigma_2 + 2\sqrt{\sigma_1\sigma_2}\cos\left(\frac{4\pi}{c} f\Delta R\right)\right]^{\frac{1}{2}} \quad . \tag{5}$$

$$R = \tfrac{1}{2}(R_1 + R_2) \qquad \Delta R \ll R$$

After square-law detection, the output signal voltage can be written

$$V_s = A\left[\sigma_1 + \sigma_2 + 2\sqrt{\sigma_1\sigma_2}\cos\left(\frac{4\pi}{c} f\Delta R\right)\right] \tag{6}$$

where A is a constant. It is variation in this voltage due to changes in f that is the intended target signature. The dependence of RCS on frequency is taken to be insignificant. For a frequency diverse bandwidth of 1%, RCS will monotonically increase by 2% over the bandwidth. The signal of interest, however, is the sinusoidal variation due to the cosine factor.

The video signal can be processed by either detecting the peak voltage or by integrating over the combined pulses; the signal dynamic range will depend on which method is used. Considering Figure 2, and assuming $\sigma_1 \geq \sigma_2$, it is seen that, for detecting the peak voltage,

$$A\sigma_1 \leq V \leq A(\sigma_1 + \sigma_2 + 2\sqrt{\sigma_1\sigma_2}) \quad . \tag{7}$$

If the dynamic range, DR, is defined as the ratio of the maximum value to the minimum value, then

92

$$DR = (1 + \sqrt{\sigma_2/\sigma_1})^2 \quad , \tag{8}$$

this ratio being independent of the amount of pulse overlap.

The dynamic range for the integrated pulse case does, however, depend on the overlap:

$$DR = \frac{\sigma_1 + \sigma_2 + 2\sqrt{\sigma_1\sigma_2}\,(1-\Delta t/T)}{\sigma_1 + \sigma_2 - 2\sqrt{\sigma_1\sigma_2}\,(1-\Delta t/T)} \quad . \tag{9}$$

For complete overlap,

$$DR = \left[\frac{1 + \sqrt{\sigma_2/\sigma_1}}{1 - \sqrt{\sigma_2/\sigma_1}}\right]^2 \tag{10}$$

which is larger than DR given in Equation (8). For $\sigma_1 = \sigma_2$, when $\Delta t > 2T/5$, sampling the peak voltage gives a larger dynamic range; for $\Delta t < 2T/5$, integration is better. In this analysis it is assumed that the pulse overlap is always large enough to make pulse integration advantageous, i.e., $\Delta t = 2\Delta R/c \ll T$.

The integrated signal voltage is then

$$V = A\left[(\sigma_1 + \sigma_2)T + 2\sqrt{\sigma_1\sigma_2}\,(T - 2\Delta R/c)\cos\left(\frac{4\pi}{c} f \Delta R\right)\right] \tag{11}$$

Equation (11) was used in a computer simulation in which the frequency was stepped in thirty-two 20 MHz increments over a 640 MHz bandwidth beginning at 142 GHz. These numbers were chosen to assess the value of adding automatic frequency diversity to a 142 GHz coherent radar currently being tested by the US Army Missile Laboratory. The radar pulse is linearly chirped (20 MHz bandwidth), so a 20 MHz increment was chosen for this analysis to assure no frequency overlap. The voltage was normalized by dividing by the largest possible value.

The simulation for the two-reflector case was designed to show: (1) how large σ_1/σ_2 may be before the effect is unmeasurable; and (2) how large or small ΔR may be before the effect is ambiguous or unmeasurable.

Figure 3 provides a reference amplitude-frequency pattern in which $\sigma_1 = \sigma_2$ and $\Delta R = 1.0$ meter. A little over four complete oscillations can be observed, with every other peak being clipped due to the relatively few number of samples taken. Voltage variations are $\pm$ 100% of the average.

(93)

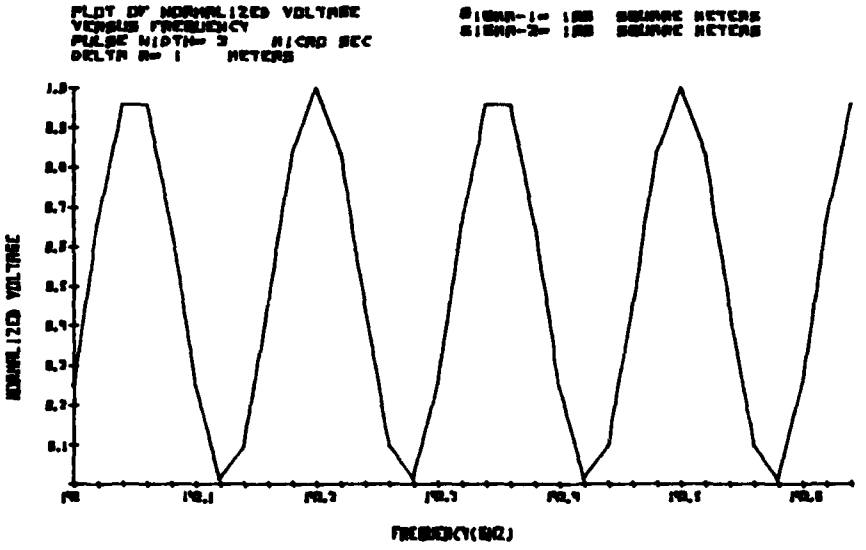

Figure 3. σ_1/σ_2=1, Range Separation = 1.0 meter.

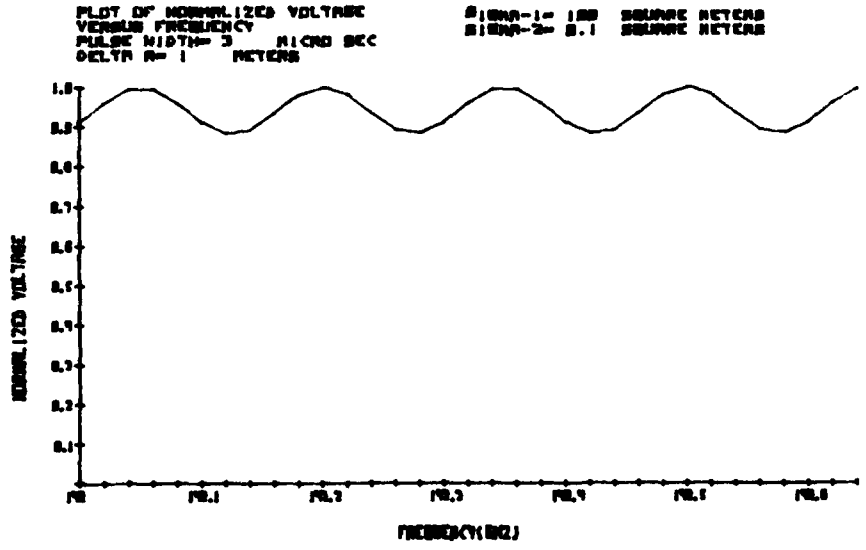

Figure 4. σ_1/σ_2=1,000, Range Separation = 1.0 meter.

(94)

In Figure 4, the simulation shows a significant voltage variation for one reflector RCS being 1,000 times larger than the other. Ratios of 10, 100, and 1,000 give voltage variations of ± 57% (5.7 dB), ± 20% (1.8 dB), and ± 6.3% (0.5 dB) respectively. Clearly, the detectability of a weak reflector in the presence of a large one is limited by radar system fluctuations, multipath, atmospheric effects, etc. Note especially that multipath may cause severe problems.

Considering different range separations, in the limit of small ΔR, the voltage variation goes to zero. If it is established, for example, that at least one-half cycle must be observable over the bandwidth, then the minimum reflector separation which provides a usable signal is about 0.1 meter. This case is shown in Figure 5.

The maximum ΔR giving an unambiguous signal is determined by the number of sampled points over the (fixed) bandwidth. At large ΔR, there are so many cycles over the bandwidth that the frequency step size does not provide enough resolution. Applying the Nyquist sampling theorem for the case of 20 MHz frequency steps, one obtains a maximum allowable ΔR of 3.75 meters. This maximum is not unreasonable for vehicle reflector separations, but if two separate targets, or perhaps one target and strong clutter, are illuminated by the radar beam, then ambiguities may occur. Figure 6 shows that the pattern for a range separation of 6.5 meters is the same as for 1.0 meter, due to the aliasing effect.

III. THREE-REFLECTOR TARGET MODEL

If a similar analysis is applied to a three-reflector target, again integrating the total received pulse, the signal voltage is found to be

$$\begin{aligned} V = A \Big[& (\sigma_1 + \sigma_2 + \sigma_3)T \\ & + 2\sqrt{\sigma_1\sigma_2}\,(T - 2\Delta R_{12}/c)\cos\left(\tfrac{4\pi}{c} f \Delta R_{12}\right) \\ & + 2\sqrt{\sigma_1\sigma_3}\,(T - 2\Delta R_{13}/c)\cos\left(\tfrac{4\pi}{c} f \Delta R_{13}\right) \\ & + 2\sqrt{\sigma_2\sigma_3}\,(T - 2\Delta R_{23}/c)\cos\left(\tfrac{4\pi}{c} f \Delta R_{23}\right)\Big] \end{aligned} \qquad (12)$$

where $\Delta R_{ij} = |R_j - R_i|$. The extension to many reflectors is

95

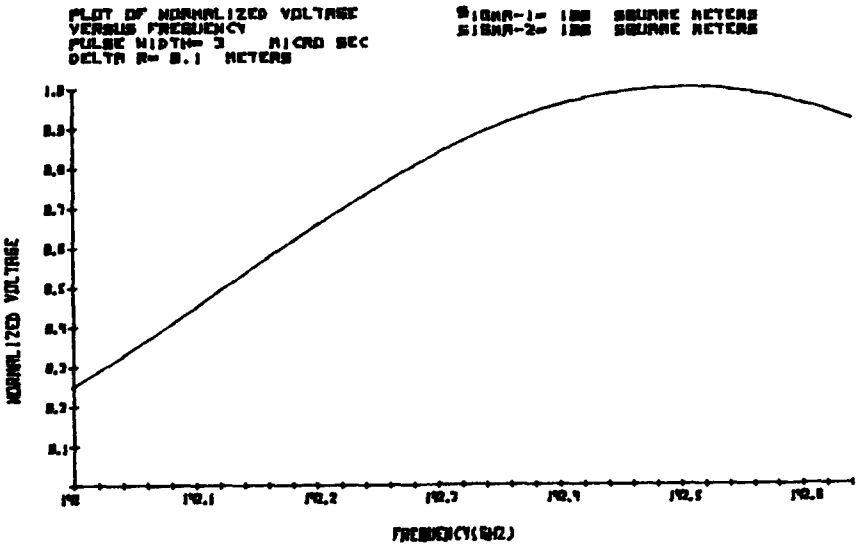

Figure 5. $\sigma_1/\sigma_2=1$, Range Separation = 0.1 meter.

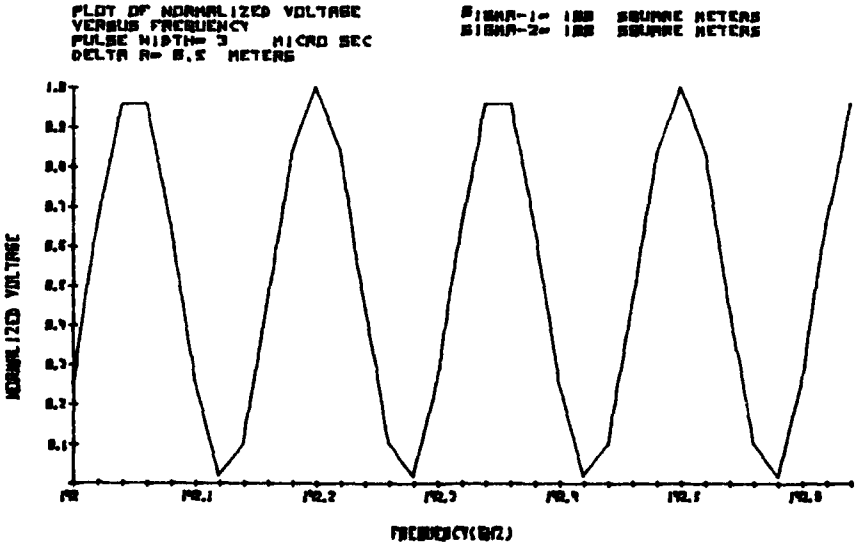

Figure 6. $\sigma_1/\sigma_2=1$, Range Separation = 6.5 meters.

(96)

clear; there will be a sinusoidal variation for each pair of reflectors on the target.

In Figures 7 and 8, the parameters have been chosen to demonstrate the complex signatures resulting from three reflectors. Possible discrimination algorithms involve using such parameters as number of peaks, peak height ratios, etc. However, the total signature information content is contained in the "spectral content" of the voltage versus frequency plot. It would seem appropriate to obtain the finite (discrete) Fourier transform of the data; then, being wary of possible aliasing, apply classification algorithms to this spectrum.

IV. THE EFFECT OF CHIRP

The analysis of Section II (two-reflectors) is now complicated by the inclusion of a linear FM chirp of 20 MHz applied to each pulse. The instantaneous frequency, f_I, of a given pulse is described by

$$f_I = f + \frac{B}{T} t \qquad 0 \le t \le T, \tag{13}$$

where f is the nominal frequency for a given frequency step, and B is the chirp bandwidth (20 MHz). The phase of the electric field intensity is then

$$\Theta = 2\pi f t + \pi \frac{B}{T} t^2 + \Theta_o \quad . \tag{14}$$

For simplicity of analysis, the t=0 point is chosen to be when the pulse returned by the nearest reflector reaches the receiver:

$$E_1^r = \frac{\sqrt{\sigma_1}\, E_o \cos(2\pi f t + \pi \frac{B}{T} t^2)}{4\pi R_1^2} \qquad 0 \le t \le T \tag{15}$$

$$E_2^r = \frac{\sqrt{\sigma_2}\, E_o \cos\left[2\pi f(t - \Delta t) + \pi \frac{B}{T} (t - \Delta t)^2\right]}{4\pi R_2^2} \tag{16}$$

$$\Delta t \le t \le T + \Delta t \; .$$

The amplitude of the square law detected voltage during pulse overlap is

$$V_s = A \left[\sigma_1 + \sigma_2 \right. \tag{17}$$

$$\left. + 2\sqrt{\sigma_1 \sigma_2} \cos\left(\frac{4\pi}{c} f \Delta R - 4\pi B(\Delta R)^2/c^2 T + \frac{4\pi}{c} \frac{B}{T} \Delta R t\right)\right].$$

(97)

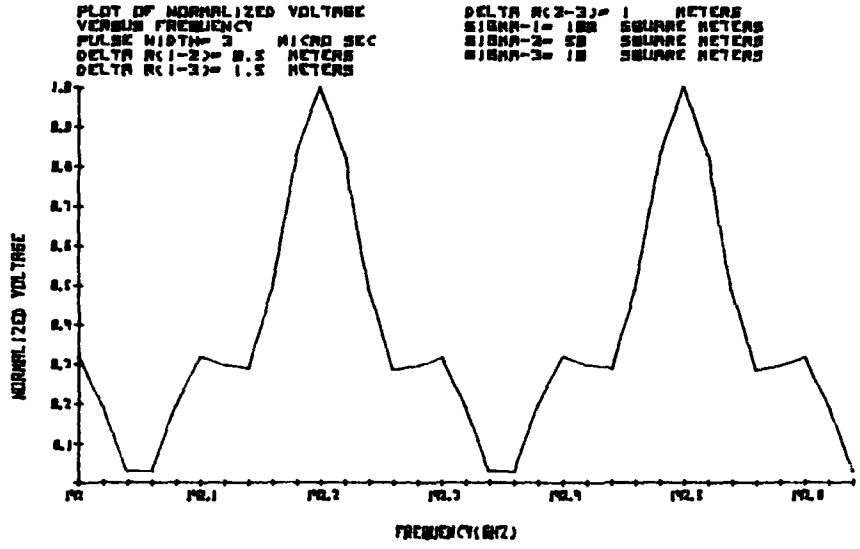

Figure 7. Three Reflector Simulation

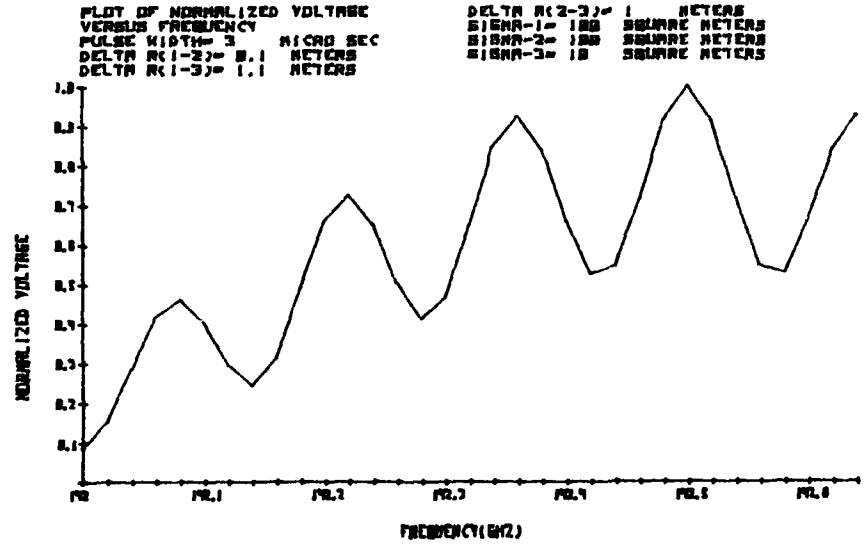

Figure 8. Three Reflector Simulation

(98)

Examining the phase of the cosine, it is seen that: the first term is the same frequency dependent factor as in Equation (6); the second term is a constant independent of frequency and time; and the third term is a time dependent phase factor which is not a function of frequency.

Using the radar parameters and ΔR=5 meters, the second term gives a phase shift of 0.02 or $(0.004(2\pi))$ radians, which is negligible. Dropping this term and integrating with respect to time over the total pulse gives

$$V = A\left[(\sigma_1 + \sigma_2)T + C\,2\sqrt{\sigma_1\sigma_2}\,(T - 2\Delta R/c)\cos\left(\frac{4\pi}{c}f\Delta R + \theta\right)\right] \quad (18)$$

$$C = \left\{2 - 2\cos\left[\frac{4\pi}{c}B\Delta R(1 - 2\Delta R/cT)\right]\right\}^{\frac{1}{2}} \Big/ \frac{4\pi}{c}B\Delta R(1 - 2\Delta R/cT) \quad (19)$$

$$\tan\theta = \frac{\cos\left(\frac{4\pi}{c}B\Delta R\right) - \cos\left[8\pi B(\Delta R)^2/c^2T\right]}{\sin\left(\frac{4\pi}{c}B\Delta R\right) - \sin\left[8\pi B(\Delta R)^2/c^2T\right]} \quad (20)$$

Comparing Equation (18) to Equation (11), one sees that the only differences are the additional phase angle θ and the amplitude factor C, both of which are independent of the nominal frequency. The effect of θ is to merely shift the amplitude versus frequency pattern. The amplitude factor C, however, can be small, resulting in insufficient sinusoidal variations. The amplitude factor is of the form

$$C = \sqrt{2 - 2\cos x} \Big/ x \quad , \quad (21)$$

and the general characteristics of this function are shown in Figure 9. For the radar parameters chosen for this analysis, at ΔR=1 meter, C=.97. For ΔR=3 meters, C=.76, which results in about a 1dB loss in the sinusoidal variation. The net effect of the chirp is a small reduction in signal variation for large separations between reflectors. Incidentally, the analysis shows that, for typical IMPATT diode characteristics (B=500 MHz, assumed linear, T=50 ns), the effects of glint due to interference are reduced to less than 25% for reflector separations larger than about 0.3 meter.

V. APPLICABILITY TO REAL TARGETS AND CLUTTER

While this paper is intended primarily to assess the feasibility of preliminary testing with simple targets, it is imperative that the technique be evaluated for real targets and clutter. In the model presented here, manmade targets are characterized by six and eight major reflectors, representing a tank and an armored personnel

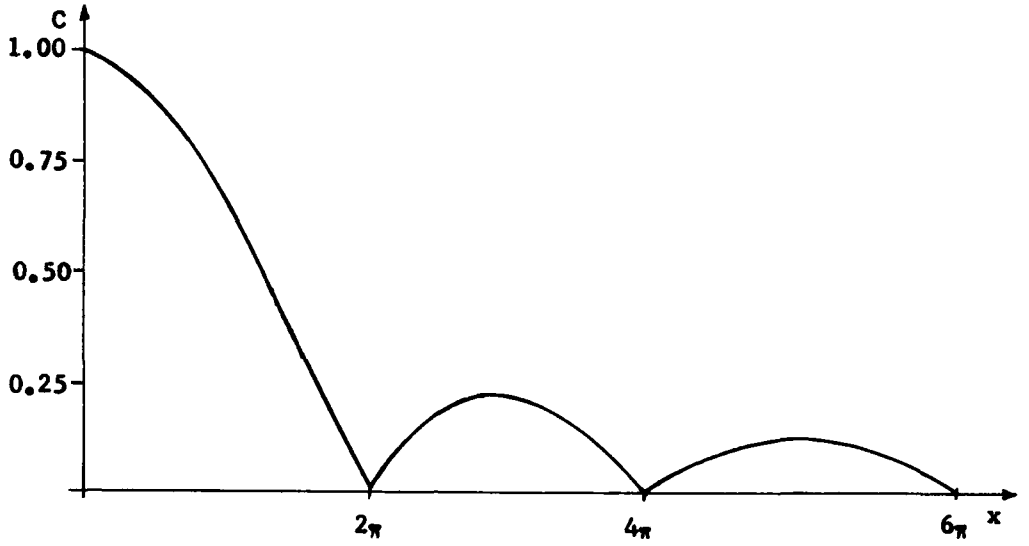

Figure 9. Amplitude Factor for a Chirped Waveform.

carrier respectively. A clutter patch of ten major reflectors representing a tree line is chosen for comparison.

From Equation (12), it is seen that each pair of reflectors provides a contribution to the Fourier transform of the data given by

$$F_{ij} = 2A\sqrt{\sigma_i\sigma_j}\,(T - 2\Delta R_{ij}/c)\cos\left[2\pi\,(2\Delta R_{ij}/c)\,f\right] \quad (22)$$

Thus, assuming infinite resolution in the Fourier transform or "frequency" domain, each pair of reflectors creates a spike of amplitude

$$A_{ij} = 2A\sqrt{\sigma_i\sigma_j}\,(T - 2\Delta R_{ij}/c) \quad (23)$$

at a "frequency" of

$$f_\Theta = 2\,\Delta R_{ij}/c \quad (24)$$

The number of contributions to the Fourier transform domain increases in an arithmetic series with the number of reflectors, although pairs with equal range separation contribute to the same spike. For n reflectors, there are $\frac{1}{2}\,n(n-1)$ contributing pairs.

Figure 10 shows the simulated Fourier transform spectra for models of a clutter patch, a tank, and an armored personnel carrier (APC). A 128 sample Fourier transform was used, allowing range

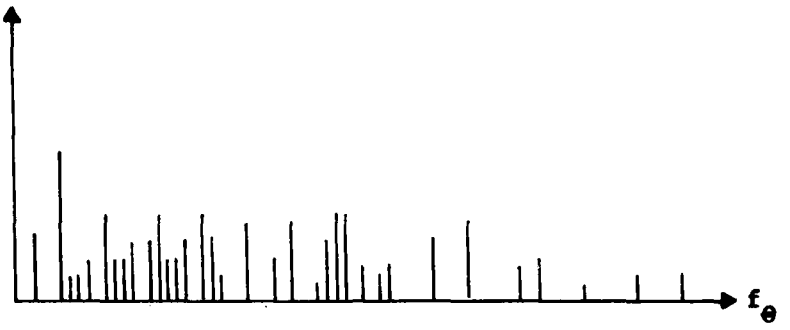

Figure 10a. Clutter Model

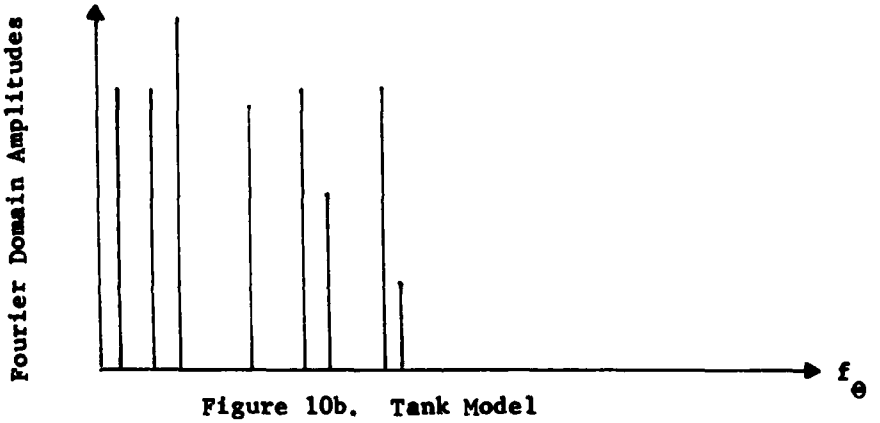

Figure 10b. Tank Model

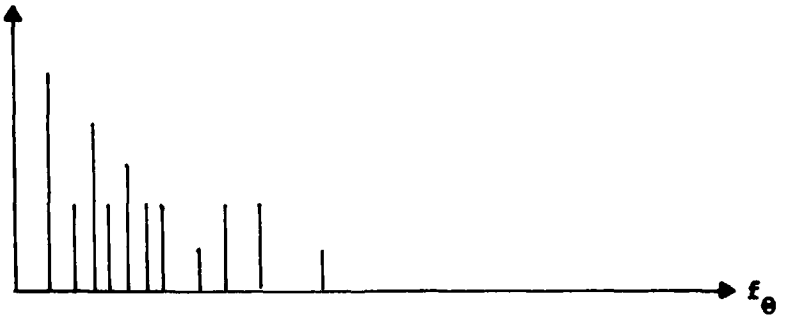

Figure 10c. APC Model

Figure 10. Fourier Domain Simulation.

(101)

separations up to 15m without aliasing.

For the clutter, the model consisted of a patch of ten trees randomly distributed over a 10 meter deep cell and having radar cross sections of 2, 5, and 10sm. For the tank model, five equally spaced road wheels (10sm) and a turret reflector (100sm) were used. The APC model consisted of six equally spaced road wheels (5sm) and two drive sprockets (2sm, 10sm).

The conclusion drawn from the simulation is that the symmetry and periodicity inherent in manmade targets distinguishes them from random natural clutter and from each other. Clearly, spikes of the same amplitude, spikes whose amplitudes are multiples of others, and uniform spacing between spikes are telltale signs of manmade targets.

VI. CONCLUSIONS

The analysis shows that the frequency diversity (frequency stepping) introduced into radar systems to reduce glint has a potential application to target/clutter discrimination and target classification for stationary targets. At a simplistic level of implementation, an experienced operator looking at the amplitude-frequency pattern could estimate the approximate size of a target. A sophisticated implementation would include microprocessor memory storage of Fourier transforms of target returns at various aspect angles to be automatically compared with the transform of an unknown response. The practical problems of implementation are the choice of diversity bandwidth (within limits) and the choice of frequency step size which will result in statistically significant Fourier components for reasonably large target or target-in-clutter data sets.

With respect to sampling, the analysis shows the desirability of increasing the number of frequency steps to 64 or 128. Using powers of two simplifies the frequency control circuit and allows data processing via the fast Fourier transform. Increasing the number of sampling points improves resolution in the transform "frequency domain" and increases the maximum allowable reflector separation. The smaller beamwidth of the millimeter radar also tends to reduce aliasing possibilities and clutter problems. Results from the three-reflector target model indicate that the most expedient data processing involves taking the discrete Fourier transforms of the amplitude-frequency patterns. Classification algorithms would then be applied to these transform spectra.

The result of using a moderately chirped waveform was found to be some signal degradation, particularly at larger reflector separations. This result is not altogether disadvantageous, since ambiguous aliased signals tend to be reduced. However, an increase in frequency steps implies a decrease in step size (fixed diversity bandwidth), and a chirp bandwidth larger that the frequency step will degrade signal resolution. It is recommended that the chirp not be used and that coherent integration of pulses be used to enhance interference effects over other fluctuations which are frequency independent.

As a final note, it should be pointed out that the complications inherent in classifying a moving target using this technique have not been considered. One might suspect, assuming that each reflector has the same radial velocity, that only a constant phase shift in the amplitude-frequency pattern would result. However, the complexities in signal amplitude variations due to target aspect angle changes and due to conical scan or monopulse tracking must also be considered.

REFERENCES:

1. N. Backmark, J. E. V. Krim, and F. Sellberg, "Frequency-agile Radar," Philips Technical Review, Vol. 28, pp. 323-328, 1967.
2. G. Lind, "Reduction of Radar Tracking Errors with Frequency Agility," IEEE Transactions on Aerospace and Electronic Systems, Vol. AES-4, pp. 410-416, May 1968.
3. R. J. Sims and E. R. Graf, "The Reduction of Radar Glint by Diversity Techniques," IEEE Transactions on Antennas and Propagation, Vol. AP-19, pp. 462-468, July 1971.
4. E. K. Reedy, J. L. Eaves, S. O. Piper, W. K. Parks, S. P. Brookshire, R. D. Wetherington, and R. N. Trebits, "Stationary Target Detection and Classification Studies (U)," Georgia Institute of Technology, Report ECOM-76-0961-2, 1978, CONFIDENTIAL.
5. P. M. Alexander and J. L. Brown, "A Preliminary Assessment of Target Classification using Noncoherent Radar Waveforms," US Army Missile Command, Technical Report T-79-80, 1979.
6. L. M. Novak, "Stationary Target Acquisition: Modeling, Prediction and Experimental Results (U)," presented at the 25th Annual Tri-Service Radar Symposium, Monterey, CA, Sept 18-20 1979, CONFIDENTIAL.
7. ———, "ARPA/TTO Program HOWLS (U)", Massachusetts Institute of Technology, Lincoln Laboratory, ESD-TR-79-218, 1979, CONFIDENTIAL.
8. L. M. Novak, "Millimeter Seeker Radar Target Acquisition Studies (U)," Proceedings of the Eighth DARPA/Tri-Service Millimeter Wave Conference, 1979, pp. 469-487, CONFIDENTIAL.